2014 IEEE International Conference on Robotics & Automation (ICRA)
Hong Kong Convention and Exhibition Center
May 31 - June 7, 2014. Hong Kong, China

# Needle Localization Using Gabor Filtering in 2D Ultrasound Images

Mert Kaya and Ozkan Bebek

*Abstract*— **In the percutaneous needle procedures using ultrasound (US) imaging, the needle should be detected precisely to avoid damage to the tissue and to get the samples from the appropriate site. Excessive artifacts and low resolution of the US images make it difficult to detect the needle and its tip. It is possible to enhance the needle image using image processing; and this work proposes a novel needle detection method in 2D US images based on the Gabor filter. This method enhances the needle outline while suppressing the other structures in the image. First, the needle insertion angle is estimated and then the needle trajectory is found with the RANSAC line estimator. The experiments with three different phantoms showed that the algorithm is robust and could work in percutaneous needle procedures using US images.**

## I. Introduction

Percutaneous needle procedures, such as biopsy and drug delivery, are commonly used in medical practices. Visibility of the needle plays an important role in the success of these procedures. Particularly in biopsies, if the needle is misplaced, erroneous samples might be collected and organs might be punctured leading to internal bleeding. In order to prevent such failures, the trajectory of the needle has to be predetermined and the needle tip should be tracked using medical imaging techniques.

Magnetic resonance imaging (MRI) provides high quality images, however custom needles are required for needle tracking since the commonly used biopsy needles are ferromagnetic. Also, MRI does not provide enough workspace for all operations. Computed Tomography (CT) and fluoroscopy imaging can be harmful due to increased dose of radiation. In addition, similar to MRI, the workspace of CT is limited. Using ultrasound (US) imaging, on the other hand, the needle can be tracked with a very small probe, and US does not have any known side effects. However, tracking the needle can be challenging due to lower image quality. US images contain undesirable artifacts and reverberation effects. Image processing algorithms can help reduce these artifacts and increase the visibility of the needle to track needle trajectory and its tip. The following summarizes the work done on developing needle localization algorithms.

Draper *et al.* [1] used variance mapping to discriminate the needle from the background. They used user defined thresholding technique and then principal component analysis (PCA) to localize needle axis and its tip. Ding *et al.* [2] used fast implementation of Hough Transform based on course-fine search to segment needle in 2D US images. Their approach decreased the computational time and can segment the biopsy needle in real time.

Okazawa *et al.* [3] used Hough transform and coordinate transform to localize curved needles under 2D US images. Rough insertion angle was supplied by the user for needle segmentation. Mathiassen *et al.* [4] used Okawaza's needle segmentation method. They measured the needle's orientation and position using an optical tracking system. From frame differences and sudden drops in image intensity, they extracted the needle tip position in real time. Ayvaci *et al.* [5] tracked the biopsy needle in 2D transrectal US images by applying second order Gaussian Filter. Prior knowledge of needle's orientation and position, image background model, and US probe stability were used to map the needle pixels in the image.

Neshat *et al* [6] modeled curved needles with Bezier polynomials. The coefficients of the polynomial were estimated using Radon Transform. In order to run the algorithm in real time, they implemented their curved needle segmentation code on a GPU. Uhercik [7] used Frangi's [8] vessel segmentation algorithm to filter lines in 3D US images. The axis of the needle was determined by a robust model fitting random sample consensus (RANSAC) algorithm. The needle tip was determined according to the sudden drop in this axis. Aboofezali [9] segmented curved needles in 3D US images using anti isotropic filter. This process reduced speckles in image and remaining speckles were reduced with a spatial contrast enhancement filter. 3D images were projected to 2D using ray casting and then Hough transform was applied to detect the curvilinear needle.

Barva *et al.* [10] localized curvilinear objects in 3D US images. 3D US images were converted to binary images with empirically determined threshold values. To localize the object, they performed least square curve fitting to the data obtained by Randomized RANSAC. Barva *et al.* [11] localized metal electrode from 3D US images. They applied thresholding and then model fitting RANSAC was applied to localize curved objects.

Novotny *et al.* [12] used passive markers to track the surgical instrument. They implemented their algorithm on a GPU, running in real time. They used a modified version of the Radon transform to detect the projection of the surgical instrument's shaft. Their GPU implementation detected the surgical instrument in 31 ms, sufficient for real time tracking. Stoll *et al.* [13] used passive markers for tracking

This work was supported by the Scientific and Technical Research Council of Turkey (TUBITAK) under Grant No. 112E312.

Mert Kaya is with Department of Electrical and Electronics Engineering, Ozyegin University, Cekmekoy, 34794 Istanbul, Turkey mert.kaya@ozyegin.edu.tr

Ozkan Bebek is with the Department of Mechanical Engineering, Ozyegin University, Cekmekoy, 34794 Istanbul, Turkey ozkan.bebek@ozyegin.edu.tr

surgical instruments in 3D US images. Markers' position were computed from 3D US image then the position and the orientation of the surgical instrument was determined. Fronheiser *et al.* [14] tracked needle with 3D color doppler US device. They vibrated the needle at high frequency with a piezoelectric buzzer. RF and color doppler filters were used to detect tip of surgical devices from US images.

Vrooijink *et al.* [15] tracked the needle in 3D using 2D US images. They used a specific pattern created by the biopsy needle in the US image known as the comet tail affect (CTA). After thresholding and morphologic operations, they found the centroid of the needle. A motorized needle insertion device was used to provide position feedback and estimate the pose of the needle tip. Chatelain *et al.* [16] tracked needles in 3D US images. They detected needles from volume intensity differences, then combined their detection method with the RANSAC and Kalman filters to track the needle more accurately.

In this study line filtering is used to develop needle localization algorithms. Specifically, the Gabor filter [17] is applied to detect the needle, which has not been used in needle localization studies with US imaging before. The Gabor filter produces much better results compared to other filtering methods because it enhances the needle's pixel better.

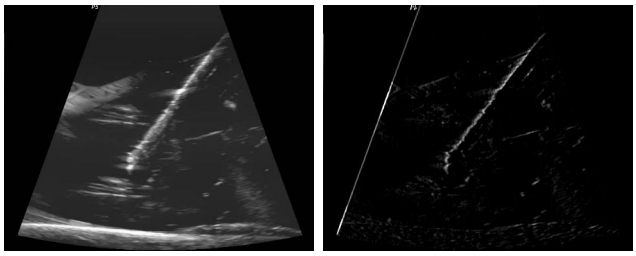

Fig. 1. 2D US image of the needle in the phantom gel. The image on the left contains the original US data and the image on the right is the output of the proposed Gabor filter.

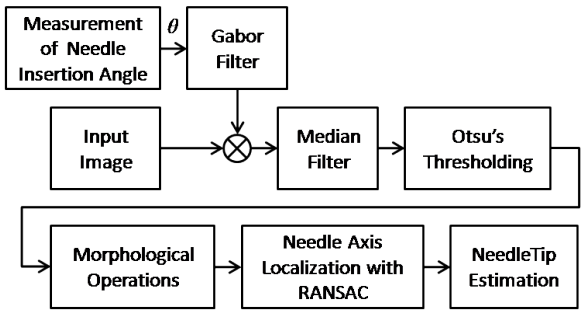


Fig. 2. Flowchart of the proposed Gabor filter based needle localization algorithm.

## II. Gabor Line Filtering Algorithm for Needle Localization

Most of the needle detection algorithms are based on the Frangi vesselness filter [8] or some empirically and adaptively determined thresholding methods. Even though the Frangi's method is one of the most common methods for segmenting vessels, it enhances all of the tubular structures in 2D and 3D US images. Therefore, it is difficult to distinguish needles from the other structures. The empirical and adaptive thresholding methods, on the other hand, are also commonly used to segment needles, however, the threshold value can vary from image to image creating discontinuities in the appearance of needle in the US image.

Due to these shortcomings of the commonly used methods, we propose a new filtering method based on the Gabor filter to detect biopsy needles in 2D US images [17]. The main difference between our filtering method and the others' is that this filter enhances the tubular structures in the direction of the needle insertion path filtering out the orthogonal structures. As a result, the needle pixels become brighter compared to the image background and the needle stands out. An imaging example using the proposed filter is shown in Fig.1.

### *The Gabor Filter*

The Gabor filter is widely used to identify fingerprint features in literature [18], and it is also used in anatomical structure detections such as liver and retina [19], [20]. The Gabor filter used in this research is adapted from [19], [20]. The method consists of three parts: (1) Gabor-based line filtering, (2) binarization, and (3) axis localization. Steps of the filtering method is shown in Fig. 2.

The 2D Gabor filter function in the spatial domain is the multiplication of complex carrier sinusoid and 2D Gaussian envelope. The 2D Gabor filter function in the spatial domain is:

$$g(x,y) = \exp\left(-\frac{x'^2+y'^2}{2\sigma^2}\right)\exp\left(j\left(2\pi\frac{x'}{\lambda}\right)\right) \quad (1)$$

where

$$\begin{aligned} x' &= x\cos\theta + y\sin\theta \\ y' &= -x\sin\theta + y\cos\theta \\ \lambda &= 0.56\sigma \end{aligned}$$

where $\sigma$ is the standard deviation value, $\lambda$ is the wavelength of modulating sinusoid and $\theta$ is the orientation of the Gabor filter.

$$e^{jx} = \cos(x) + j\sin(x) \quad (2)$$

Using (2), the 2D Gabor filter can be rewritten as:

$$\begin{aligned} Re\{g(x,y)\} &= exp(-\frac{x'^2+y'^2}{2\sigma^2})\cos(2\pi\frac{x'}{\lambda}) \quad (3) \\ Im\{g(x,y)\} &= exp(-\frac{x'^2+y'^2}{2\sigma^2})\sin(2\pi\frac{x'}{\lambda}) \end{aligned}$$

The line filtered image $I_g(x,y)$ is the convolution of the input image $I(x,y)$ and the imaginary part of the Gabor filter kernel $Im\{g(x,y)\}$ as in (4).

$$I_g(x,y) = I(x,y) * Im\{g(x,y)\} \quad (4)$$

## III. Estimation of Needle Insertion Angle

The Gabor filter is applied in accordance with the orientation angle, $\theta$. In order to localize the biopsy needle in US images, the orientation of the filter has to be equal to the insertion angle of the needle because the best appearance of the needle and its tip can be obtained at this angle value. Therefore, this filtering angle is consistent with the needle insertion angle. In Fig. 4, the Gabor filter is applied to the same image by changing the orientation angle in increments of 30°. This image bank shows that the needle visibility is maximized when the filter orientation angle is almost equal to the needle insertion angle, and the artifacts in the image created by other structures are minimized.

The angle estimation is divided into two cases base on prior knowledge. When frame sequences are used prior knowledge is available for the frames; when a single frame is used such data are not available. Two different techniques are proposed below to estimate the needle insertion angles for both cases.

*1) Estimation of the Needle Insertion Angle from a single US image:* Estimating insertion angle value in an image is quite complicated unless the angle is known a priori. We developed a method based on the quadrants of cartesian coordinate system to estimate the needle insertion angle in 2D US images. With this method, a rough estimate of the insertion angle, $\alpha$, is chosen first as shown in Fig. 3(b). If the needle trajectory is similar to the trajectories as shown in quadrants I and III, we choose the initial insertion angle, $\alpha$, as 135°, and for the quadrants II and IV, we choose $\alpha$ as 225°. After the initial assignment, the Gabor filter is applied with the estimated insertion angle. The needle trajectory becomes more clear and in the next step the RANSAC line estimator is applied, and slope of the line, $m$, is found. The exact insertion angle in terms of the Gabor filter coordinate system, $\theta$, can be found more precisely at this point and then it can be used in the Gabor filter again to localize the biopsy needle.

Due to the nature of how US images are collected, the coordinate frames of the needle axis and the Gabor filter are not positioned in the same direction, as shown in Fig. 3(a). Using (5), the exact insertion angle value is expressed in terms of the Gabor filter coordinate system.

$$\theta = \alpha + \mid \tan^{-1}(m) \mid -45° \tag{5}$$

Steps of the needle insertion angle estimation is depicted in Fig. 5 for two different types of gel phantom. First, raw images are collected ((a) and (f)). Second, a rough estimate of the insertion angle is chosen and the Gabor filter is applied ((b) and (g)). Next, the RANSAC line estimator is applied to get the exact insertion angle, $\theta$ ((c) and (h)). Finally, the Gabor and the RANSAC are repeated to localize the needle and its tip ((d-e) and (i-j)).

*2) Estimation of the Needle Insertion Angle in Frame Sequences:* In US image sequences (videos), the needle insertion angle can be determined at the beginning of needle penetration and can be assumed constant afterwards.

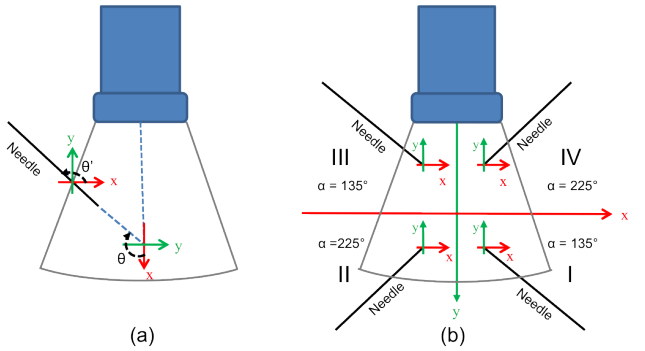


Fig. 3. The US and needle coordinate systems. (a) Angle $\theta$ is shown. (b) Possible $\alpha$ angles are shown for the quadrants.

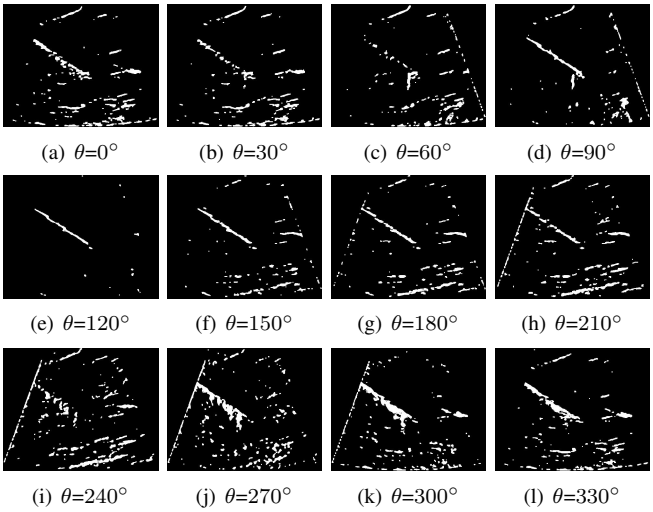


Fig. 4. The output of the Gabor filter bank using the proposed line filter. The raw image in Fig.7(a) is used. The orientation angle, $\theta$, is changed in 30° increments to show the filtering effects.

Therefore, the needle insertion angle, $\theta$, is determined before filtering is applied. The differences in close frames can be used to estimate the insertion angle. In general, the image acquisition speed of the US devices are 30 frames per second (fps). Two images that are one second apart can be used for angle estimation assuming that the displacement of the US probe is zero at the beginning of the needle insertion and the tissue (phantom) doesn't move, as shown in (6).

$$I_n = I[kn] - I[k(n-1)] \tag{6}$$

where $I$ is the input image, $I_n$ is the difference image, k is the frame step, and n = 1,2,3,... is the frame number. This process generates a bank of binary images. The needle insertion angle is updated as data are collected. Initially, we used the least square method to detect the insertion angle by fitting a line to needle pixels. However, due to the artifacts in the image differences, the error in the angle estimation increased dramatically. We observed that the needle pixels obtained from the frame difference images lie in the maximum variance region. Therefore, the principal component analysis is used to get the best insertion angle.

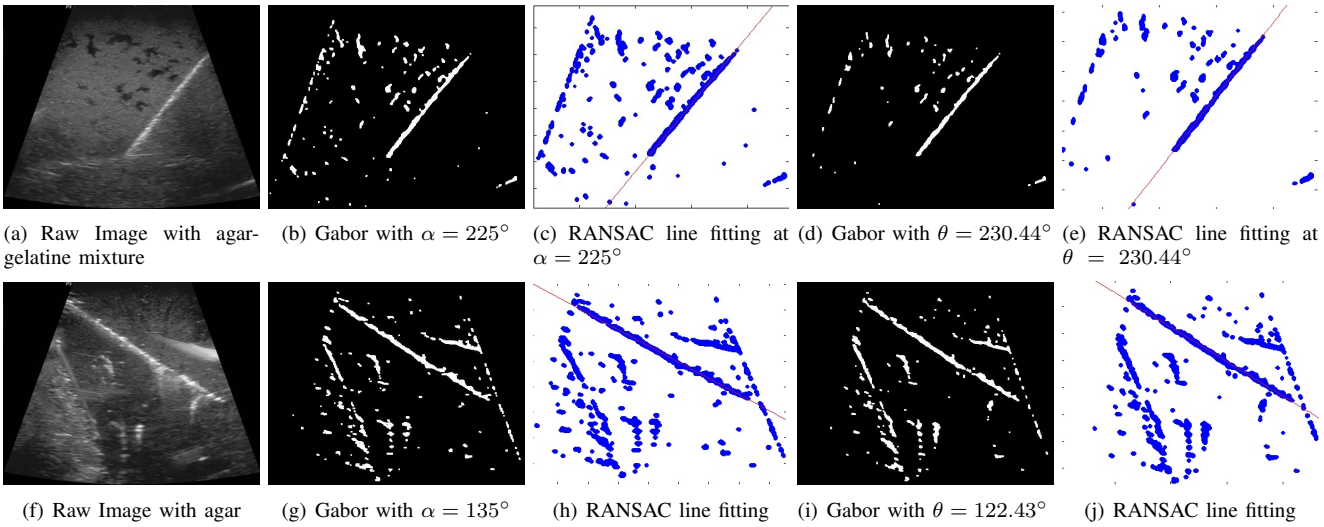

(a) Raw Image with agar-gelatine mixture (b) Gabor with $\alpha = 225°$ (c) RANSAC line fitting at $\alpha = 225°$ (d) Gabor with $\theta = 230.44°$ (e) RANSAC line fitting at $\theta = 230.44°$

(f) Raw Image with agar (g) Gabor with $\alpha = 135°$ (h) RANSAC line fitting (i) Gabor with $\theta = 122.43°$ (j) RANSAC line fitting

Fig. 5. The order for the needle insertion angle estimation and detection in 2D US images. (a) The raw image of the needle in agar-gelatin based phantom. (b) Gabor filter applied with estimated insertion angle $\alpha = 225°$. (c) RANSAC to determine needle axis. (d) Gabor filter applied at exact insertion angle $\theta = 230.44°$. (e) RANSAC line fitting to localize the needle and its tip. (f) The raw image of the needle in agar based phantom. (g) Gabor filter applied with estimated insertion angle $\alpha = 135°$. (h) RANSAC to determine needle axis. (i) Gabor filter applied at exact insertion angle $\theta = 122.43°$. (e) RANSAC line fitting to localize the needle and its tip.

Then, covariance matrix of PCA is calculated as:

$$\Sigma = \begin{bmatrix} \sigma_{xx}^2 & \sigma_{xy}^2 \\ \sigma_{yx}^2 & \sigma_{yy}^2 \end{bmatrix} \tag{7}$$

where

$$\sigma_{xy}^2 = \frac{\sum_{i=1}^{N}(x_i - \bar{x})(y_i - \bar{y})}{N} \tag{8}$$

and $x_i$ and $y_i$ are coordinates of the white pixels in the binary image, $\bar{x}$ and $\bar{y}$ are the means of $x_i$ and $y_i$, respectively, and N is the number of the white pixels in the sum of difference images. Then, the corresponding eigenvector $\upsilon$ in this direction is:

$$\upsilon = \begin{bmatrix} \upsilon_{(1,1)} & \upsilon_{(1,2)} \\ \upsilon_{(2,1)} & \upsilon_{(2,2)} \end{bmatrix} \tag{9}$$

The angle of major principal axis, $\theta_m$, in this direction is:

$$\theta_m = \left( -\tan^{-1}\left( -\frac{\upsilon_{(2,1)}}{\upsilon_{(1,1)}} \right) \right) \tag{10}$$

The needle insertion angle equals to the sum of the major principal axis in this direction and $\pi$. Since the result of $\tan^{-1} \in [-\pi, \pi]$, $\pi$ is added to $\theta_m$ for the Gabor filter to work:

$$\theta = \theta_m + \pi. \tag{11}$$

Steps of the needle insertion angle estimation for frame sequences is shown in Fig. 6. Two images that are 30 frames apart in a sequence are chosen. These images are binarized and their difference is obtained (Fig. 6(c)). Then, in order to detect the needle insertion angle, Gabor filter followed by RANSAC line fitting is applied (Fig. 6(d-e)).

## IV. Image Binarization

After the Gabor-based line filtering, image binarization is required for line fitting. Binarization is achieved in three steps: smoothing, thresholding, and removing small particles. The steps are explained in detail below.

*1) Median Filtering:* After the Gabor-based line filtering is applied, the output image contains considerable noise (Fig. 7(b)), and the image should be smoothen for thresholding operations. Therefore, a median filter is used to smoothen the image and reduce the noise. 7×7 sized kernel was used for images and for frame sequences. In addition, this median filter enhances the needle edges. The output of the median filter is shown in Fig. 7(c).

*2) Automatic Thresholding:* Thresholding is required to get an outline of the needle but we observed that the threshold value is not constant after the median filter is applied. Therefore, an automatic thresholding method was needed. To determine the threshold value, Otsu's thresholding method [21] was used. For difference image of close frames, the automated thresholding value was used directly. However, threshold value obtained by Otsu's method can binarize excessive number of pixels as foreground for single images because of low intensity level of needle pixels and artifacts. In this point, RANSAC algorithm can fail. In order to prevent failure of RANSAC algorithm and increase the success rate of the method, Otsu's threshold value was multiplied with a tuned constant which was selected between 2 and 4. As shown Fig. 7(d) and Fig. 6(c), this method can successfully distinguish the needle pixels.

*3) Morphologic Operations:* After automatic thresholding operations, a 3×3 square shaped structuring element morphologic erosion and dilation is applied. After thresholding, the noise is reduced with morphologic erosion. Even though morphologic erosion reduces the noise, it deteriorates the

(a) Frame number = 96 (b) Frame number = 126 (c) Frame Difference Image (d) Gabor with $\theta = 135.34°$ (e) RANSAC Line Fitting

Fig. 6. The order for the needle insertion angle estimation and detection in 2D US frame sequences. (a) and (b) are raw images of the needle in agar-based phantom. (c) The difference image after the binarization process. Smoothing, thresholding, and morphologic operations are applied respectively. (d) Gabor filter applied at estimated insertion angle, $\theta = 135.34°$. (e) The RANSAC line fitting to localize the needle.

continuity of the needle. Morphologic dilation is applied in order to enhance the needle structure, and improve the needle continuity. The result of morphologic operations is shown in Fig. 7(e).

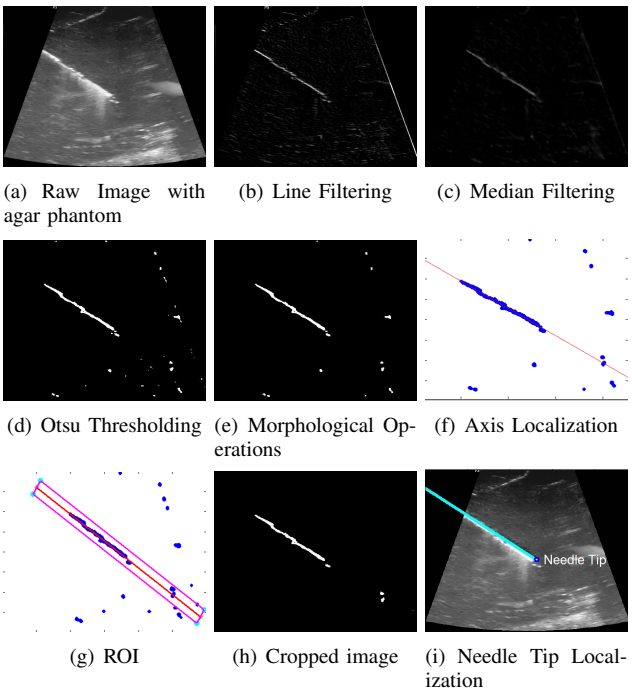


(a) Raw Image with agar phantom (b) Line Filtering (c) Median Filtering

(d) Otsu Thresholding (e) Morphological Operations (f) Axis Localization

(g) ROI (h) Cropped image (i) Needle Tip Localization

Fig. 7. (a) Raw image acquired from agar-based phantom, (b) Gabor filter based line filtering when $\theta$=119°, (c) median filtering, (d) thresholding with Otsu's method, (e) morphological erosion and dilation, (f) axis localization with RANSAC, (g) region of interest (ROI) when $N = 6$, (h) ROI image, and (i) localize needle axis and tip.

## V. Needle Axis Localization

### A. Random sample consensus (RANSAC)

The needle direction is found using the RANSAC algorithm which is a robust line estimator. In the proposed algorithm, the Gabor filter enhances the needle in the US images and decreases the continuity of the other structures. Therefore, the RANSAC can effectively distinguish between the needle outline and the more apparent needle image.

### B. Region of Interest

After the needle trajectory was found, a region of interest (ROI) was selected around the needle pixels to increase the effectiveness of the needle tip detection. This also decreased the computation time. The coordinates of the ROI was calculated as:

$$\begin{aligned} width &= x_2 - x_1 \\ height &= y_2 - y_1 \\ length &= \sqrt{width^2 + height^2} \\ (x_s, y_s) &= \left(\frac{N \times height}{2 \times length}, \frac{N \times width}{2 \times length}\right) \\ (x_f, y_f) &= (x_1 - x_s, y_1 + y_s) \\ (x_{sec}, y_{sec}) &= (x_1 + x_s, y_1 - y_s) \\ (x_{th}, y_{th}) &= (x_2 + x_s, y_2 - y_s) \\ (x_{ft}, y_{ft}) &= (x_2 - x_s, y_2 + y_s) \end{aligned} \quad (12)$$

where $(x_1, y_1)$, $(x_2, y_2)$ are coordinates of the needle trajectory obtained by the RANSAC; $(x_s, y_s)$ are translation distances according to the original coordinate position; $(x_f, y_f)$, $(x_{sec}, y_{sec})$, $(x_{th}, y_{th})$, and $(x_{ft}, y_{ft})$ are the coordinates of the rectangular ROI; $N$ is the thickness of the ROI in terms of pixels. The ROI was depicted as a rotated rectangle in Fig. 7(g).

### C. Needle Tip Detection

The output of the binarized Gabor filter image was cropped according to the ROI process explained above. The largest chunk in this image is the needle and its sharp edge is the needle tip. An intact needle outline is not always guaranteed at the end of this process. In these cases the needle pixels are seen as fragmented needles which makes it difficult to distinguish the needle from the other structures. To separate the needle from the artifacts, the distances between the divided groups were calculated. The chunk that is the farthest from the others is the far end of the needle and sharp edge of this outline is the needle tip. An example needle tip detection is given in Fig. 7(i).

## VI. Experiments

### A. Experimental Setup

*1) The US Machine:* The images were acquired using a LOGIQ P5 2D US machine (General Electric, USA), with a linear 2D US probe (11L, General Electric, USA). The acquired images were 640 × 480 pixels.

*2) Phantom:* Three different types of phantoms were used during the needle insertion experiments. These were gelatin-based (1 L water + 80 g gelatin powder) (Fig. 1), agar-based (1 L water + 20 g agar + 5 ml chlorhexidine) (Fig.5.a and

Fig. 7.a), and gelatin and agar mixture (1 L water + 40 g gelatin powder + 10 g agar + 2.5 ml chlorhexidine) (Fig. 5.f) phantoms. These phantoms were prepared according to the recipe given in [22]. The phantoms were prepared and let to rest eight hours before the experiments to eliminate excessive air bubbles. In the experiments, 22 gauge biopsy needles were used.

### B. Experimental Results

*1) Execution Time:* The algorithm was implemented in MATLAB and run on a 64-bit Window 7 workstation, which has an Intel Xeon E5-2620 CPU running at 2 GHz and 32 GB of RAM. 164 US images were used in trials. The image sizes were 640×480 pixels. In all of the images, the needle trajectory was localized successfully. The execution time of the proposed line filter method for a single image is 0.234 $\pm$ 0.023 seconds (mean $\pm$ standard deviation). We are expecting much faster execution times, about five folds if the algorithm is implemented to run on a GPU.

*2) Results:* In this study, 149 single ultrasound images, and 15 frame sequences were used to evaluate the algorithm. Three different types of phantoms were used to check the algorithms capability to detect the needles in different contrast levels and images with excessive extraneous structures.

For each image, Gabor filter banks with $1^\circ$ increments were generated. With these images, the results of the initial needle insertion angle estimation were checked. In all of the images, the algorithm successfully detected the needle insertion axis and the needle tip. During the experiments a goniometer was used to measure the needle insertion angle manually with respect to the upright held ultrasound probe. Comparable angle measurement results were obtained from the proposed algorithm.

In this study, by mimicking real tissues, phantoms were used specifically to prove that the proposed method can work in a variety of US images which have distinct backgrounds. Both heterogenous and homogenous types of phantoms were fabricated to perform the proposed method in different kinds of mediums. In the fabrication process, cylindrical structures made from latex and spherical glass balls in various sizes placed inside the phantoms randomly. In addition, some of the phantom gels were directly cooled. Hence, they contain air bubbles. During the imaging, despeckle filters of the US machine were closed. Therefore, the images contain different types of artifacts, such as mirror and reverberation artifacts. In the acquired images, needle was suppressed by the artifacts. In many of the images, the intensity level of needle pixels were very close to the image background, and also; the needle was not seen as a complete structure. The algorithm was able to detect and localize the biopsy needle in all of the phantoms confirming the robustness of the method.

## REFERENCES


[1] K. J. Draper, C. C. Blake, L. Gowman, D. B. Downey, and A. Fenster, "An algorithm for automatic needle localization in ultrasound-guided breast biopsies," *Medical Physics*, vol. 27, no. 8, pp. 1971–1979, 2000.

[2] M. Ding and A. Fenster, "A real-time biopsy needle segmentation technique using hough transform," *Medical Physics*, vol. 30, no. 8, pp. 2222–2233, 2003.

[3] S. H. Okazawa, R. Ebrahimi, J. Chuang, R. N. Rohling, and S. E. Salcudean, "Methods for segmenting curved needles in ultrasound images," *Medical Image Analysis*, vol. 10, no. 3, pp. 330 – 342, 2006.

[4] K. Mathiassen, D. Dall Alba, R. Muradore, P. Fiorini, and O. Elle, "Real-time biopsy needle tip estimation in 2d ultrasound images," in *Proceedings of the IEEE International Conference on Robotics and Automation (ICRA)*, no. 2. IEEE Robotics and Automation Society, May 2013, pp. 4348–4353.

[5] A. Ayvaci, P. Yan, S. Xu, S. Soatto, and J. Kruecker, "Biopsy needle detection in transrectal ultrasound," *Computerized Medical Imaging and Graphics*, vol. 35, pp. 653 – 659, 2011.

[6] H. Neshat and R. Patel, "Real-time parametric curved needle segmentation in 3d ultrasound images," in *Biomedical Robotics and Biomechatronics, 2008. BioRob 2008. 2nd IEEE RAS EMBS International Conference on*, 2008, pp. 670–675.

[7] M. Uhercik, J. Kybic, C. Cachard, and H. Liebgott, "Line filtering for detection of microtools in 3d ultrasound data," in *Ultrasonics Symposium (IUS), 2009 IEEE International*, 2009, pp. 594–597.

[8] A. Frangi, W. Niessen, K. Vincken, and M. Viergever, "Multiscale vessel enhancement filtering," in *Medical Image Computing and Computer-Assisted Interventation MICCAI98*. Springer Berlin Heidelberg, 1998, vol. 1496, pp. 130–137.

[9] M. Aboofazeli, P. Abolmaesumi, P. Mousavi, and G. Fichtinger, "A new scheme for curved needle segmentation in three-dimensional ultrasound images," in *Proceedings of the Sixth IEEE international conference on Symposium on Biomedical Imaging: From Nano to Macro*, ser. ISBI'09, 2009, pp. 1067–1070.

[10] M. Barva, J. Kybic, J. Mari, C. Cachard, and V. Hvalac, "Automatic localization of curvilinear object in 3d ultrasound images," in *SPIE International Symposium Medical Imaging*, San Diego, California, USA, Feb 2005.

[11] ——, "Localizing metal electrode from 3d ultrasound data using r-ransac and intensity priors," in *EMBEC'05*, Prague, Czech Republic, 2005.

[12] P. M. Novotny, J. A. Stoll, N. V. Vasilyev, P. J. del Nido, P. E. Dupont, and R. D. Howe, "Gpu based real-time instrument tracking with three dimensional ultrasound," in *Proceedings of the 9th international conference on Medical Image Computing and Computer-Assisted Intervention - Volume Part I*, 2006, pp. 58–65.

[13] J. Stoll, H. Ren, and P. Dupont, "Passive markers for tracking surgical instruments in real-time 3-d ultrasound imaging," *Medical Imaging, IEEE Transactions on*, vol. 31, no. 3, pp. 563–575, 2012.

[14] M. Fronheiser, S. Idriss, P. Wolf, and S. Smith, "Vibrating interventional device detection using real-time 3-d color doppler," *Ultrasonics, Ferroelectrics and Frequency Control, IEEE Transactions on*, 2008.

[15] G. Vrooijink, M. Abayazid, and S. Misra, "Real-time three-dimensional flexible needle tracking using two-dimensional ultrasound," in *Proceedings of the IEEE International Conference on Robotics and Automation (ICRA)*, no. 2. IEEE Robotics and Automation Society, May 2013, pp. 1680–1685.

[16] P. Chatelain, A. Krupa, and M. Marchal, "Real-time needle detection and tracking using a visually served 3d ultrasound probe," in *Proceedings of the IEEE International Conference on Robotics and Automation (ICRA)*, no. 2. IEEE Robotics and Automation Society, May 2013, pp. 1668–1673.

[17] I. Fogel and D. Sagi, "Gabor filters as texture discriminator," *Biological Cybernetics*, vol. 61, no. 2, pp. 103–113, 1989.

[18] C.-J. Lee and S.-D. Wang, "Fingerprint feature extraction using gabor filters," *Electronics Letters*, vol. 35, no. 4, pp. 288–290, 1999.

[19] C. Vicas, M. Lupsor, R. Badea, and S. Nedevschi, "Detection of anatomical structures on ultrasound liver images using gabor filters," in *Automation Quality and Testing Robotics (AQTR), 2010 IEEE International Conference on*, vol. 2, 2010, pp. 1–5.

[20] R. Rangayyan, F. Oloumi, F. Oloumi, P. Eshghzadeh-Zanjani, and F. Ayres, "Detection of blood vessels in the retina using gabor filters," in *Electrical and Computer Engineering, 2007. CCECE 2007. Canadian Conference on*, 2007, pp. 717–720.

[21] N. Otsu, "A Threshold Selection Method from Gray-level Histograms," *IEEE Transactions on Systems, Man and Cybernetics*, vol. 9, no. 1, pp. 62–66, 1979.

[22] J. W. Li, M. K. Karmakar, X. Li, W. H. Kwok, and W. D. N. Kee, "Gelatin-agar lumbosacral spine phantom: A simple model for learning the basic skills required to perform real-time sonographically guided central neuraxial blocks," *Journal of Ultrasound in Medicine*, vol. 30, no. 2, pp. 263–272, 2011.